Appl. Sci. **2015**, *5*, 695-705; doi:10.3390/app5040695

OPEN ACCESS

applied sciences

ISSN 2076-3417

www.mdpi.com/journal/applsci

Article

Characterization of Transition Metal Oxide/Silicon Heterojunctions for Solar Cell Applications

Luis G. Gerling *, Somnath Mahato †, Cristobal Voz, Ramon Alcubilla and Joaquim Puigdollers

Electronic Engineering Department, Polytechnic University of Catalonia, Barcelona 08034, Spain; E-Mails: som.phy.ism@gmail.com (S.M.); cristobal.voz@upc.edu (C.V.); ramon.alcubilla@upc.edu (R.A.); joaquim.puigdollers@upc.edu (J.P.)

† Current Address: Department of Applied Physics, Indian School of Mines, Dhanbad 826004, India

* Author to whom correspondence should be addressed; E-Mail: guillermo.gerling@upc.edu; Tel.: +34-93-401-1002; Fax: +34-93-401-6756.

Academic Editor: Alejandro Pérez-Rodríguez

Received: 15 September 2015 / Accepted: 1 October 2015 / Published: 10 October 2015

Abstract: During the last decade, transition metal oxides have been actively investigated as hole- and electron-selective materials in organic electronics due to their low-cost processing. In this study, four transition metal oxides (V_2O_5, MoO_3, WO_3, and ReO_3) with high work functions (>5 eV) were thermally evaporated as front p-type contacts in planar n-type crystalline silicon heterojunction solar cells. The concentration of oxygen vacancies in MoO_{3-x} was found to be dependent on film thickness and redox conditions, as determined by X-ray Photoelectron Spectroscopy. Transfer length method measurements of oxide films deposited on glass yielded high sheet resistances (~10^9 Ω/sq), although lower values (~10^4 Ω/sq) were measured for oxides deposited on silicon, indicating the presence of an inversion (hole rich) layer. Of the four oxide/silicon solar cells, ReO_3 was found to be unstable upon air exposure, while V_2O_5 achieved the highest open-circuit voltage (593 mV) and conversion efficiency (12.7%), followed by MoO_3 (581 mV, 12.6%) and WO_3 (570 mV, 11.8%). A short-circuit current gain of ~0.5 mA/cm^2 was obtained when compared to a reference amorphous silicon contact, as expected from a wider energy bandgap. Overall, these results support the viability of a simplified solar cell design, processed at low temperature and without dopants.

Keywords: transition metal oxides; silicon heterojunction solar cells; vanadium oxide; molybdenum oxide; tungsten oxide; rhenium oxide

1. Introduction

Although crystalline silicon (c-Si) solar cells are a mature technology with competitive energy prices in several markets, efforts toward higher efficiencies, lower costs and lesser environmental impacts continue to lead the photovoltaic community. State of the art technology already allows for low-temperature deposition of dopants (T < 200 °C) in amorphous silicon a-Si:H/c-Si heterojunction devices, but thermally-diffused doping (T > 900 °C) is still the industry standard, covering ~12% of the module fabrication energy input [1]. As advanced solar cell architectures become closer to the theoretical efficiency limits for single-junction devices, further cost reduction must then come from ambient-temperature or solution-based processes and materials.

In parallel, the development of thin-film and dye-sensitized/organic photovoltaics has introduced novel materials with excellent optoelectronic properties that could substitute standard silicon dopants. Such materials have recently been reported in conjunction with p- and n-type c-Si, including organic polymers (PEDOT:PSS [2], P3HT [3]), transparent conductive oxides (ZnO [4]), transition metal oxides (TiO_2 [5], MoO_3 [6], WO_3 [7]) or their combination [8,9], reaching power conversion efficiencies as high as 18.8%[10] for MoO_3/n-type c-Si heterojunctions. A distinctive attribute of these materials is their preferential conductivity for one kind of charge carrier (*i.e.*, holes) while blocking the other kind (electrons), aiding in the separation of photogenerated carriers [11]. They are usually wide bandgap semiconductors (highly transparent) with low contact resistivities, although the primary benefit is their processability by low-temperature techniques (vacuum thermal evaporation, atomic layer deposition) or by thin-film coating methods.

This paper explores the use of four transition metal oxides (V_2O_5, MoO_3, WO_3, and ReO_3) as front p-type contacts in planar n-type crystalline silicon (n-Si) solar cells. The compositional, optical and electrical properties of these oxides will be discussed in terms of the solar cell design, making emphasis on their advantages (optical gains) and disadvantages (post-annealing degradation) when compared to conventional a-Si:H layers.

2. Experimental Details

The oxide/c-Si solar cells were fabricated on double-side polished mono-crystalline (float zone, 100 orientation) n-Si wafers (~2.5 Ωcm, $N_D \sim 1.8 \times 10^{15}$ cm^{-3}) of 280 μm thickness. After the standard RCA cleaning process and 1% HF bath (1 min) to remove native SiO_2, samples were introduced in a Plasma-Enhanced Chemical Vapor Deposition (PECVD) system (Elettrorava, Turin, Italy) for deposition of three hydrogenated amorphous-silicon carbide layers (a-SiC_x:H, $0.2 < x < 1$) on the rear side of the wafer. This passivating/n^+ doped/reflective stack was then laser-fired (infrared nanosecond laser) to create a matrix of point contacts (0.5% contacted area) with a measured contact resistivity <0.5 mΩcm^2 and an effective surface recombination velocity ~50 cm/s (before metallization) [12]. After a second 1% HF bath, the different transition metal oxides (Sigma Aldrich, Dorset, England;

99.99%, powdered) were deposited by vacuum thermal evaporation from a tantalum boat at <8 × 10^{-6} mbar at a rate <0.2 Å/s. Even though ReO_3 was evaporated without difficulty, the film proved unstable when exposed to ambient air and some of the devices could not be measured. The oxide thickness was fixed at 15 nm and controlled by quartz microbalance. The samples were then briefly exposed to air for transferring into a RF-magnetron sputtering system for deposition of an 80 nm Indium-Tin Oxide (ITO) conductive/anti-reflective layer (ITO target: J.J. Lesker, Hastings, England), followed by lithographic patterning of 1 cm^2 cell area. Contacting of the rear side was done by electron-beam assisted evaporation of Ti (15 nm)/Al (1000 nm) followed by a front grid (4.3% shadow) of thermally evaporated Ag (metals: J.J. Lesker, Hastings, England). A reference device was also fabricated by replacing the transition metal oxide layer with an intrinsic (i) a-Si:H (4 nm)/(p) a-Si:H (15 nm) stack contacted by ITO and using the same point contact strategy on the rear side. Figure 1(a) depicts the structure of the oxide/n-Si heterojunction solar cells.

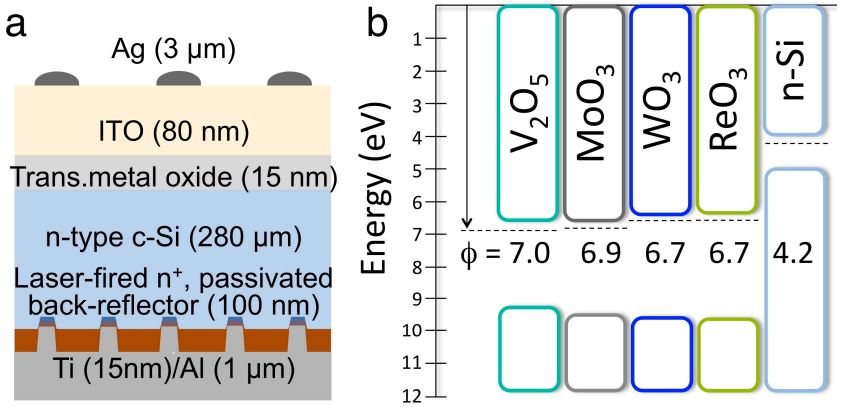

Figure 1. (**a**) Schematic of the transition metal oxide/n-Si heterojunction solar cell; (**b**) reported work functions for ReO_3 [13], V_2O_5, MoO_3 and WO_3 [14]. The valence and conduction band energy levels of c-Si are also shown.

Characterization of the solar cells was performed before and after a 10 min 160 °C annealing in N_2 atmosphere. The current-voltage characteristics were measured (Keithley Instruments 2601B, Cleveland, OH, USA) both in dark and AM1.5g standard illumination (Oriel Instruments, Irvine, CA, USA), extracting the relevant cell performance parameters. The External Quantum Efficiency (EQE) response was measured by a commercial instrument (PV Measurements QEX10, Boulder, CO, USA) and the total reflectance by spectrophotometry (Shimadzu 3600, Kyoto, Japan) with an integrating sphere. Optical simulation of the solar cell structure was done by the tool *Wafer Ray Tracer* [15] (Version 1.6.4, PV Lighthouse Pty. Ltd., Australia) at 20 nm intervals and 5000 incident rays. Transfer Length Method (TLM) measurements of the oxide films (15 nm thick) were also performed with 1 × 0.1 cm Au electrodes at various distance intervals, measuring the current-voltage response (Keithley Instruments 2636, Cleveland, OH, USA; 1fA resolution) in the dark and under vacuum. The elemental composition of MoO_3 films was determined from Gaussian-Lorentzian peak fittings of X-ray Photoelectron Spectroscopy (XPS) spectra measured at <3 × 10^{-9} mbar using a non-monochromatic Al-Kα source (SPECS, Berlin, Germany; Phoibos 150 detector).

3. Results and Discussion

3.1. Transition Metal Oxide Characterization

Transition metal oxides are wide bandgap semiconductors that have been employed as hole and electron transport layers in organic solar cells and light emitting diodes due to their wide range of work functions varying from 3 eV (ZrO_2) to 7 eV (V_2O_5) [16]. Their doping character is determined by defect vacancies in their atomic structure, resulting in either p-type doping for metal vacancies or in n-type doping for oxygen vacancies, as is the case in the four n-type oxides under study (Figure 1(b)) [13,14]. Likewise, the conductivity and work function vary with oxygen content in an inverse manner, shifting from high work function insulators (MoO_3) to semiconductors (MoO_{3-x}) to low work function metallic-like conductors (MoO_2) as the cation oxidation state decreases ($Mo^{+6} \rightarrow Mo^{+5} \rightarrow Mo^{+4}$) [16]. In order to determine the stoichiometry of the prepared samples, Figure 2 shows the elemental content of Mo^{+6} and Mo^{+5} cations calculated from the integrated areas of the fitted Mo 3d XPS peaks (inset) for different MoO_3 thicknesses and two different post-deposition treatments (air-exposure and UV-ozone, 15 min). For the air-exposed films, it is observed that the Mo^{+6} content increases with film thickness and stabilizes at a value of ~94%, while the Mo^{+5} content inversely decreases to ~6%. This phenomenon has been thoroughly investigated for several metallic substrates and has been attributed to thermodynamically driven redox reactions at the MoO_x/substrate interface [17]. Similarly, the UV-ozone treated samples follow the same trend but with a larger Mo^{+6} content due to ozone oxidation, stabilizing at a value of ~96% (~4% for Mo^{+5}). By integrating the fitted O 2p peaks, average oxygen to metal (O/M) ratios were calculated at $MoO_{2.5}$ (air-exposed) and $MoO_{2.6}$ (UV-ozone). Oxygen deficiency has also been reported for thermally evaporated V_2O_5 [18], WO_3 [7] and ReO_3 [13], which allows for fine-tuning of the desired work function by means of different process conditions and post-deposition treatments [19,20].

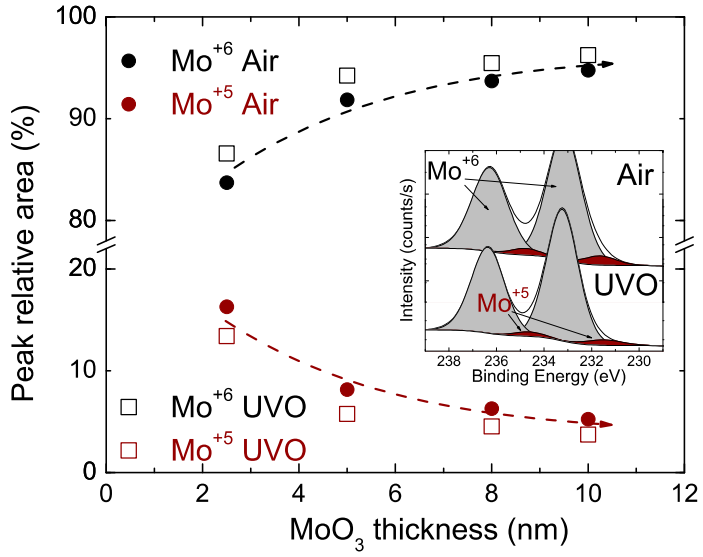

Figure 2. Relative content of Mo^{+6} and Mo^{+5} oxidation states for different MoO_3 film thicknesses (2.5, 5, 8 and 10 nm) and post-deposition treatments (air exposure and ultraviolet light ozone—UVO). Inset shows the fitted XPS spectra for both Mo 3d states identified (8 nm). Lines are a guide to the eye.

Even if variations in composition allow for enhancements in conductivity, transition metal oxides are in general poor conductors when compared to doped silicon or transparent conductive oxides. To determine the electrical properties of the evaporated MoO_3 films, the Transfer Length Method (TLM) results were analyzed to extract the sheet resistance (R_{sh}), both in glass and n-Si substrates, according to the relation [21]:

$$R_T = 2R_C + \left(\frac{R_{Sh}}{W}\right)d \quad (1)$$

where R_T is the total resistance measured between two electrodes of width W separated by a distance d, while $2R_C$ is the transversal contact resistance between Au/MoO_3 (glass sample) and Au/MoO_3/n-Si (n-Si sample). Figure 3 plots the dark R_T measurements at increasing d intervals for both samples, obtaining a sheet resistance of ~5 × 10^{12} Ω/sq for MoO_3/glass and ~1 × 10^4 Ω/sq for MoO_3/n-Si. The large difference between both measurements is explained by the formation of an inversion layer on silicon's surface, acting as p-type contacts in the n-Si substrate [10,22]. Note also that R_{sh} for the n-Si substrate (with ~2.5 Ωcm resistivity) is ~65 Ω/sq and does not contribute significantly to the inversion layer resistance. Similar results were obtained for V_2O_5 and WO_3 deposited on glass and n-Si substrates (Table 1), indicating the formation of an inversion layer. Also, MoO_3 samples yielded a 3% higher R_{sh} when treated with UV-ozone, as expected from a higher Mo^{+6} content.

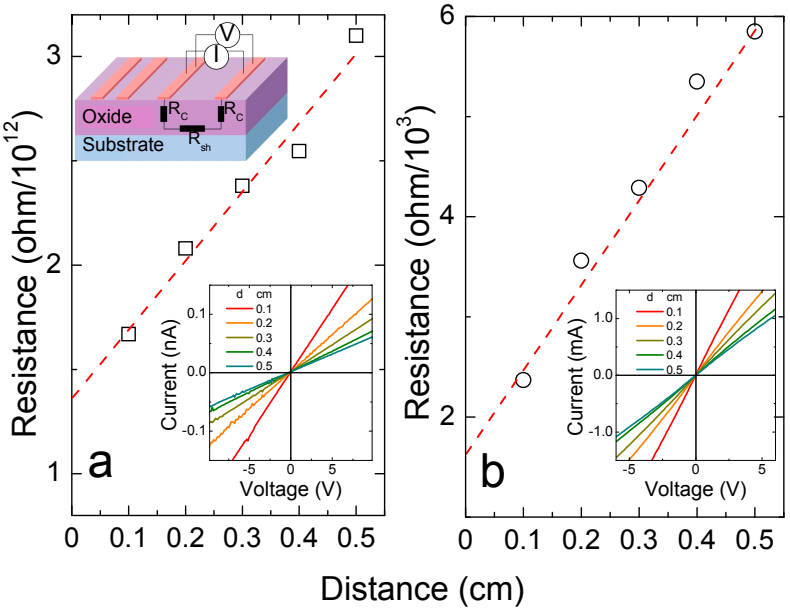

Figure 3. Transfer length method measurements of 15 nm thick MoO_3 films deposited on (**a**) glass and (**b**) n-Si, measured with 40 nm Au electrodes. Insets show the current-voltage measurements at different distance intervals d.

Due to the high sheet resistance values discussed above, a transparent conductive oxide is required for current collection, so that the main contribution of the inversion layer (IL) to the cell series resistance comes from the transversal current flow across the IL/oxide/ITO interfaces, which can be approximated from the contact resistivity $\rho_C = R_C A_T$ (where A_T is the effective current flow area). However, the obtained contact resistivities were overestimated due to the large errors inherent to the TLM itself [21], being inconsistent with the series resistances and fill factors measured in the finished solar cells and needing further analysis.

Table 1. Sheet resistance (R_{sh}) of the oxides calculated from the transfer length method (TLM). The ReO_3 device was not measured due to film instabilities.

Oxide	Sheet Resistance (R_{sh}), Ω/sq	
	Glass substrate	Silicon substrate
V_2O_x	3.3×10^9	5.8×10^3
MoO_x	5×10^{12}	1.0×10^4
WO_x	1.1×10^9	1.2×10^5

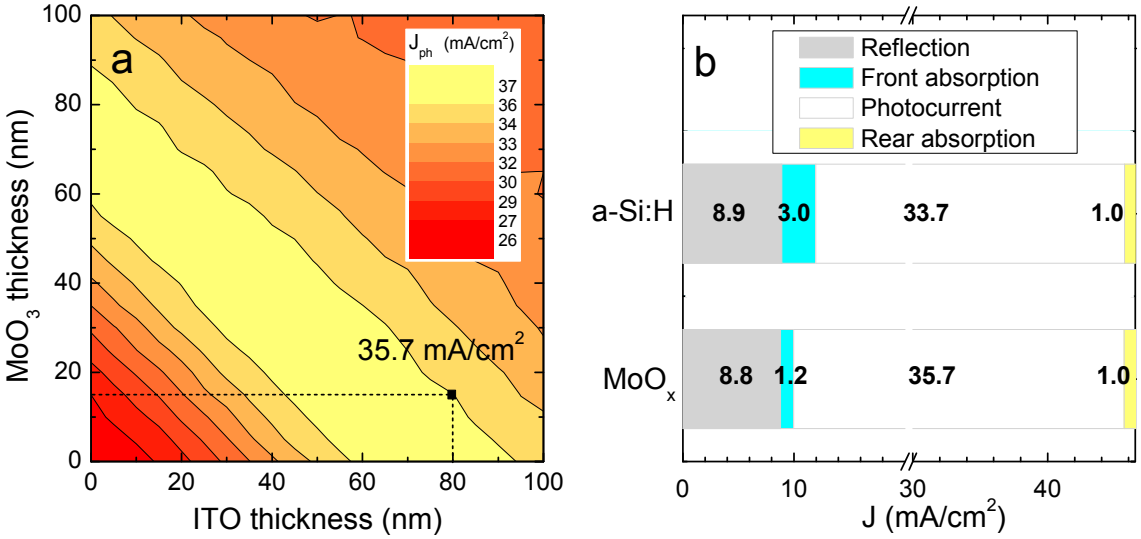

Figure 4. (**a**) Simulated photocurrent density (J_{ph}) of the planar solar cell as a function of MoO_3 and Indium-Tin Oxide (ITO) layer thickness, achieving a maximum photocurrent of 35.7 mA/cm^2 for 80 nm ITO and 15 nm MoO_3. (**b**) Simulated optical losses (in mA/cm^2) for MoO_x and a-Si:H (15 nm each).

From the optical perspective, the thicknesses of both ITO and transition metal oxide layers need to be adjusted for an optimum anti-reflection quality. Figure 4(a) shows the maximum photocurrent density J_{ph} for the MoO_3/n-Si solar cell simulated with the *Wafer Ray Tracer* program (AM1.5g solar spectrum), showing an optimum window across the 0–100 nm thickness range. The simulation parameters (refractive index and extinction coefficient) where wavelength dependent and taken from the program material database [15], including MoO_3 (alpha-phase) from [23]. Since the sputtered ITO has a moderately high R_{sh} ~130 Ω/sq, a minimum thickness of 80 nm was fixed in order to limit the resistance losses, yielding a maximum photocurrent of 35.7 mA/cm^2 for a MoO_3 thickness of 15 nm. This oxide thickness also ensures a uniform coverage of the random pyramids. Furthermore, the large bandgap energy of transition metal oxides (E_{gap} ~3 eV) reduces the absorption losses in comparison to standard a-Si:H (~1.7 eV). Figure 4(b) shows the distribution of the incident current density for both MoO_3 and a-Si:H as front window layers, showing the optical losses by reflection and by parasitic absorption (front and rear layers). The larger MoO_3 E_{gap} represents a potential gain in photocurrent of ~1.8 mA/cm^2, although reflection losses are considerably high and could be lowered to <2.7 mA/cm^2 if a texturized wafer is used.

3.2. Solar Cell Characterization

Besides reduced parasitic absorption and moderate resistance losses, transition metal oxides must also generate a potential difference that facilitates the separation of photogenerated carriers. Figure 5 depicts the current density-voltage (*J-V*) characteristic of the oxide/n-Si solar cells under standard AM1.5g illumination and in the dark (inset). All oxide solar cells show the typical rectifying behavior of a p-n junction except for ReO_3, whose surface quality was severely deteriorated and produced a Schottky diode between ITO and silicon. The cell dark response at high voltage shows larger series resistance (R_S) than the a-Si:H reference, while at low voltage the so-called recombination diode indicates inadequate passivation of the oxide/n-Si interface. Under illumination, the highest open-circuit voltage (V_{OC}) is achieved by the V_2O_5 cell with 593 mV, followed by MoO_3 (581 mV) and WO_3 (570 mV). These V_{OC} values are notable given the chemical dissimilarity between materials, the thinness of the oxide layer and the simple solar cell design, and even though higher V_{OC} s have been reported by use of (i) a-Si:H passivating interlayers [7,10], they introduce an additional processing step (PEVCD). Moreover, a correlation could be inferred between the reported work functions values (Figure 1(b)) and the measured V_{OC} s (with larger work functions exerting a stronger surface inversion on n-Si), but further research is necessary. As to the short-circuit current densities (J_{SC}), all cells achieved a relatively constant value of ~29 mA/cm^2, with the reference being slightly lower due to its higher parasitic absorption (lower E_{gap}). The observed Fill Factors (*FF*) were similar for all cells (>70%) and could be improved by decreasing R_S, which is dominated by ITO's sheet resistance and probably by the high contact resistivity amongst n-Si/oxide/ITO. By considering the obtained solar cell parameters (Table 2), the Power Conversion Efficiencies (*PCE*) were 12.7% (V_2O_5), 12.6% (MoO_3) and 11.8% (WO_3), compared to a reference 13.1%.

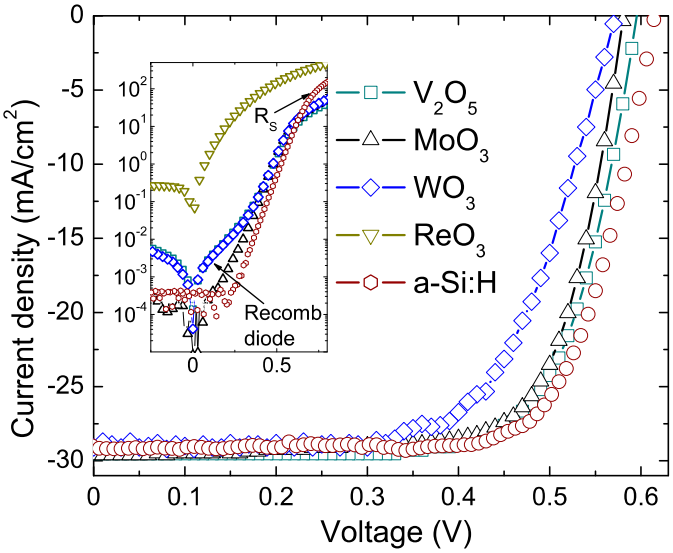

Figure 5. Current density-voltage (*J-V*) response of the fabricated oxide/n-Si solar cells under standard AM1.5g illumination, including an a-Si:H reference device. Inset shows *J-V* under dark conditions.

Table 2. Performance parameters of the fabricated oxide/n-Si solar cells and the a-Si:H reference device.

Oxide	*PCE* %	V_{OC} mV	J_{SC} mA/cm^2	*FF* %	R_S Ωcm^2
V_2O_5	12.7	593	29.6	72.4	0.9
MoO_3	12.6	581	29.6	73.1	0.8
WO_3	11.8	570	29.1	71.0	1.0
ReO_3	3.1	245	28.9	44.4	1.1
a-Si:H	13.1	617	29.1	73.0	0.55

The External Quantum Efficiency (EQE) response of the solar cells is shown in Figure 6. The curves show considerable reflectance losses in the ultraviolet and near-infrared wavelengths, which could be lowered by fabricating the device on a texturized wafer. Likewise, the reflectance minimum (~750 nm) could be shifted to shorter wavelengths by reducing the ITO thickness, matching the solar spectrum power peak (~525 nm) and enhancing photon absorption. A notable feature of the oxide cells is the improved response in the 300–550 nm range when compared to a-Si:H, explained by the lower parasitic absorption of the oxide films and predicted by the optical simulation of the device, accounting for a net gain in J_{SC} of ~0.5 mA/cm^2.

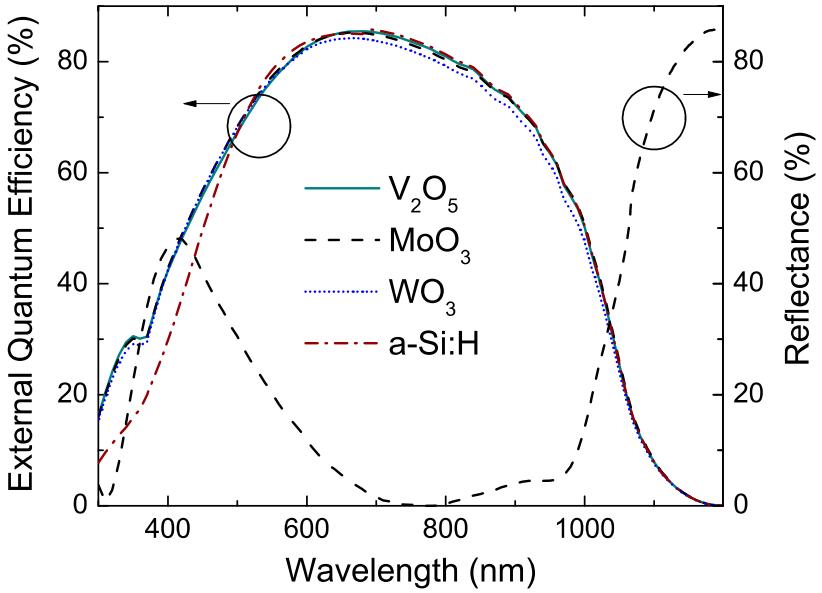

Figure 6. External quantum efficiency and total reflectance of the fabricated oxide/n-Si solar cells, including an a-Si:H reference device.

Finally, it is well known in a-Si:H/c-Si heterojunction technology that ion bombardment occurring during ITO sputtering degrades the passivation of a c-Si surface [24], increasing carrier recombination (lower J_{SC}) and decreasing the effective minority carrier lifetime (lower V_{OC}). A short post-fabrication annealing at 160 °C is sufficient to recover the damage, as evidenced by a V_{OC} and J_{SC} enhancement of the reference a-Si:H cell to 645 mV and 32.7 mA/cm^2. In search of a similar boost in performance, the oxide/n-Si cells were annealed under the same conditions, obtaining varied results as summarized in Figure 7. The V_2O_5 device decreased its *PCE* to 10.8% as a consequence of a drop in *FF*, even though

its V_{OC} indeed recovered to 614 mV. For the MoO_3 cell, its efficiency dropped to 11.0% due to V_{OC} (560 mV) and J_{SC} (27.6%) deterioration. The WO_3 cell was the only material that showed a positive improvement in efficiency (12.6%), increasing its V_{OC} and J_{SC} to 583 mV and 30 mA/cm^2. Overall, the results suggest that the V_2O_5 and MoO_3 films are strongly sensitive to temperature, although the threshold at which their optical and electric properties degrade still needs to be determined.

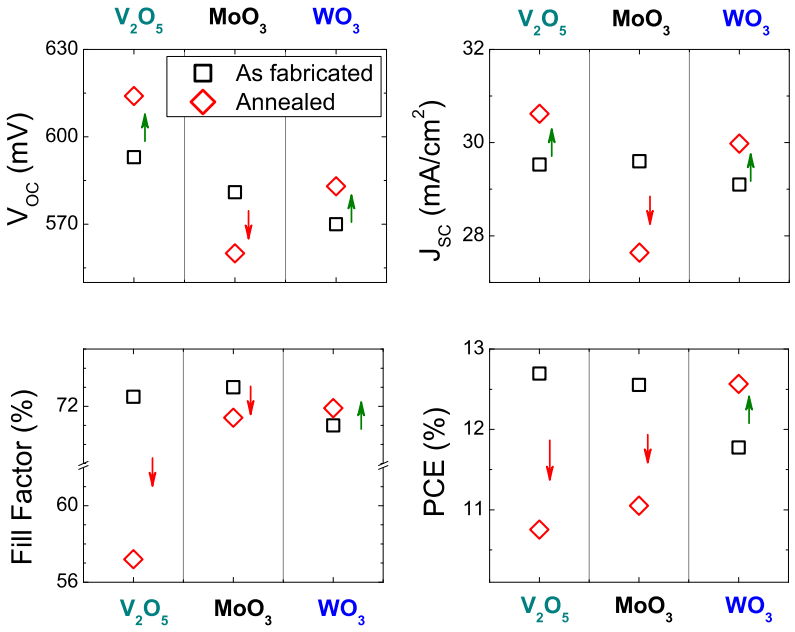

Figure 7. Solar cell performance parameters before and after thermal annealing (10 min, 160 °C).

4. Conclusions

Thermally evaporated transition metal oxides were successfully employed as front p-type contacts in planar n-type c-Si solar cells, achieving V_{OC} values of 593 mV (V_2O_5), 581 mV (MoO_3) and 570 mV (WO_3), for a maximum power conversion efficiency of 12.7% (V_2O_5). XPS analyses of MoO_3 films showed a dependence of the cation oxidation state with thickness and an average oxygen deficiency of $MoO_{2.55}$, while moderate sheet resistance values (10^4 Ω/sq) of the oxide films deposited on n-Si were attributed to the formation of a surface inversion layer. When compared to a reference a-Si:H layer, a gain in J_{SC} ~0.5 mA/cm^2 was seen for the wider bandgap oxide layers, though serious losses in efficiency were observed for the V_2O_5 and MoO_3 cells after thermal annealing treatments. Future studies should focus on enhancing the passivation of the oxide/c-Si interface, avoiding the damage caused by ITO sputtering and lowering the contact resistivity. Lastly, by use of another transition metal oxide layer as rear n-type contact, a simplified solar cell architecture that is dopant-free and fully processed at low temperature could offer important reductions in cost for crystalline silicon photovoltaics.

Acknowledgments

This work was supported by the Spain government under the ENE2013-48629-C4-1-R and ENE2014-56237-C4-1-R projects. The authors would like to thank Thomas Duc (École Polytechnique, Paris) for the optical simulations and the transfer length method measurements, Montserrat Domínguez

for the X-ray photoelectron spectroscopy analyses and Anna Morales-Vilches for the reference solar cell. The authors are also thankful for financial support from the Mexican government grants program (CONACyT) and the Erasmus Mundus Action 2 Areas+ grants program.

Author Contributions

L.G.G., C.V. and J.P. conceived and designed the experiments; L.G.G. and S.M. performed the experiments and analyzed the data; R.A. coordinated the equipment and materials; L.G.G. wrote the paper.

Conflicts of Interest

The authors declare no conflict of interest.

References

1. Alsema, E.A.; de Wild-scholten M.J. Environmental impacts of crystalline silicon photovoltaic module production. In Proceedings of the 13th CIRP International Conference in Life Cycle Engineering, Leuven, Belgium, 31 May 2006.
2. Thomas,J.P.; Leung, K.T. Defect-minimized PEDOT: PSS/planar-Si solar cell with very high efficiency. *Adv. Funct. Mater.* **2014**, *24*, 4978–4985.
3. Weingarten, M.; Zweipfennig, T.; Vescan A.; Kalisch, H. Low-temperature processed hybrid organic/silicon solar cells with power conversion efficiency up to 6.5%. *MRS Proceedings* **2015**, *1771*, mrss15-2133323.
4. Hussain, B.; Ebong, A.; Ferguson, I. Zinc oxide as an active n-layer and antireflection coating for silicon based heterojunction solar cell. *Sol. Energy Mater. Sol. Cells* **2015**, *139*, 95–100.
5. Nagamatsu, K.A.; Avasthi, S.; Sahasrabudhe, G.; Man, G.; Jhaveri, J.; Berg, A.H. Titanium dioxide/silicon hole-blocking selective contact to enable double-heterojunction crystalline silicon-based solar cell. *Appl. Phys. Lett*. **2015**, *106*, 123906.
6. Bullock, J.; Yan, D.; Cuevas, A.; Wan, Y.; Samundsett, C. n- and p-type silicon solar cells with molybdenum oxide hole contacts. *Energy Procedia* **2015**, *77*, 446–450.
7. Bivour, M.; Temmler, J.; Steinkemper, H.; Hermle, M. Alternative contact materials for induced junction silicon solar cells. *Sol. Energy. Mater. Sol. Cells* **2015**, *142*, 34–41.
8. Liu, R.; Lee, S.T.; Sun, B. 13.8% efficiency hybrid Si/organic heterojunction solar cells with MoO_3 film as antireflection and inversion induced layer. *Adv. Mater*. **2014**, *26*, 6007–6012.
9. Mu, X.; Yu, X.; Xu, D.; Shen, X.; Xia, Z.; He, H. High efficiency organic/silicon hybrid solar cells with doping-free selective emitter structure induced by a WO_3 thin interlayer. *Nano Energy* **2015**, *16*, 54–61.
10. Battaglia, C.; de Nicolás, S.M.; de Wolf, S.; Yin, X.; Zheng, M.; Ballif, C. Silicon heterojunction solar cell with passivated hole selective MoO_x contact. *Appl. Phys. Lett*. **2014**, *104*, 113902.
11. Würfel, P. *Physics of Solar Cells*, 1st ed.; Wiley-VCH: Weinheim, Germany, 2005; pp. 113–114.

12. Colina, M.; Morales-Vilches, A.; Voz, C.; Martin, I.; Ortega, P.R.; Alcubilla, R. Low surface recombination in silicon-heterojunction solar cells with rear laser-fired contacts from aluminum foils. *IEEE J. Photovoltaics* **2015**, *5*, 805–811.
13. Yoo, S.J.; Chang, J.H.; Lee, J.H.; Moon, C.K.; Wu, C.I.; Kim, J.J. Formation of perfect ohmic contact at indium tin oxide/N,N'-di(naphthalene-1-yl)-N,N'-diphenyl-benzidine interface using ReO_3. *Sci. Rep.* **2014**, *4*, 3902.
14. Meyer, J.; Hamwi, S.; Kröger, M.; Kowalsky, W.; Riedl, T.; Kahn, A. Transition metal oxides for organic electronics: Energetics, device physics and applications. *Adv. Mater*. **2012**, *24*, 5408–5427.
15. Wafer Ray Tracer simulation tool, Version 1.6.4, PV Lighthouse Pty. Ltd., Australia. Available online: http://www.pvlighthouse.com.au (accessed on 1 June 2015).
16. Greiner, M.T.; Chai, L.; Helander, M.G.; Tang, W.-M.; Lu, Z.-H. Transition metal oxide work functions: The influence of cation oxidation state and oxygen vacancies. *Adv. Funct. Mater*. **2012**, *22*, 4557–4568.
17. Greiner, M.T.; Chai, L.; Helander, M.G.; Tang, W.-M; Lu, Z.-H. Metal/metal-oxide interfaces: How metal contacts affect the work function and band structure of MoO_3. *Adv. Funct. Mater.* **2013**, *23*, 215–226.
18. Zilberberg, K.; Trost, S.; Meyer, J.; Kahn, A.; Behrendt, A.; Lützenkirchen-Hecht, D. Inverted organic solar cells with sol-gel processed high work-function vanadium oxide hole-extraction layers. *Adv. Funct. Mater.* **2011**, *21*, 4776–4783.
19. Irfan, I; Ding, H.; Gao, Y.; Small, C.; Kim, D.Y.; Subbiah, J.; So, F. Energy level evolution of air and oxygen exposed molybdenum trioxide films. *Appl. Phys. Lett.* **2010**, *96*, 243307.
20. Shi, X.B.; Xu, M.F.; Zhou, D.Y.; Wang, Z.K.; Liao, L.S. Improved cation valence state in molybdenum oxides by ultraviolet-ozone treatments and its applications in organic light-emitting diodes. *Appl. Phys. Lett.* **2013**, *102*, 233304.
21. Meier, D.L.; Schroder, D.K. Contact resistance: Its measurement and relative importance to power loss in a solar cell. *IEEE Trans. Electron Devices* **1984**, *31*, 647–653.
22. Bullock, J.; Cuevas, A.; Allen, T.; Battaglia, C. Molybdenum oxide MoO_x: A versatile hole contact for silicon solar cells. *Appl. Phys. Lett.* **2014**, *105*, 232109.
23. Lajaunie, L.; Boucher, F.; Dessapt, R.; Moreau, P. Strong anisotropic influence of local-field effects on the dielectric response of α-MoO_3. *Phys. Rev. B* **2013**, *88*, 115141.
24. Illiberi, A.; Kudlacek, P.; Smets, A.H.M.; Creatore, M.; van de Sanden, M.C.M. Effect of ion bombardment on the a-Si:H based surface passivation of -Si surfaces. *Appl. Phys. Lett.* **2011**, *98*, 242115.